Supplemental Material

Charge quenching at defect states in transition metal dichalcogenide–graphene van der Waals heterobilayers

Daniel Hernangómez-Pérez,[1] Andrea Donarini,[2] and Sivan Refaely-Abramson[1]

[1] *Department of Molecular Chemistry and Materials Science, Weizmann Institute of Science, Rehovot 7610001, Israel*

[2] *Institute of Theoretical Physics, University of Regensburg, 93040 Regensburg, Germany*

Email: daniel.hernangomez@weizmann.ac.il

Keywords: 2D materials, transition-metal dichalcogenides, van der Waals, defects, graphene, transport, single-electron

CONTENTS

I. COMPUTATIONAL DETAILS

Our *ab initio* calculations were performed using density functional theory as implemented in the QUANTUM ESPRESSO package[1]. For the exchange-correlation functional, we used the non-empirical generalized gradient approximation of Perdew-Burke-Ernzerhof[2]. We employed a plane-wave basis set and scalar relativistic (full relativistic for the spin-orbit coupling calculations) norm-conserving pseudopotentials[3] with a basis cut-off of 95 Ry for WS_2–Gr and 90 Ry for MoS_2–Gr. The self-consistent charge density was calculated within a $6\times6\times1$ grid and the total energy considered to be converged when the difference between iterations was smaller than a threshold value of 10^{-9} Ry. Preoptimizations of the supercell were performed with VASP[4], using LDA as exchange correlation functional, a basis energy cut-off of 600 eV and a $6\times6\times1$ **k**-grid. Additional relaxations in the presence of the vacancy were performed by fixing the supercell lattice vectors and optimizing the position of the atoms during the self-consistent field cycle until all the components of the ionic forces were smaller than 10^{-3} Ry/a_0. For the optimization procedure we also employed the van-der Waals corrected functional `vdw-df-09`[5,6] to account for potential additional changes in the interlayer separation.

II. ELEMENTS OF APPLIED GROUP THEORY

For the sake of completeness, we briefly summarize in section of the Supporting Information (SI) elementary point-group theory results that underlay the density functional theory findings and the calculation of the single-particle tunneling rate matrix in the main paper and Sec. III of the SI. We follow here Refs. 7–9. In the absence of the graphene layer, the XS_2 TMDC layer with a chalcogen vacancy possesses C_{3v} symmetry, the point-group of the equilateral triangle. This point group is characterized by a proper rotation axis of order 3 and 3 planes of symmetry. Traditionally, E, $C_3^{\pm}$ and σ_v ($v=1,2,3$) are chosen as notation for the identity, rotation and reflection elements of the group, defining three equivalence classes (see scheme in Fig. S1).

As a consequence of Schur's lemmas[8], the eigenvalues and eigenstates of a Hamiltonian which commutes with all symmetry operators $\hat{G}$ of a group can be classified according to the irreducible represetations of the group itsself. This is the case, if and only if, the group

is a complete group of invariance. In other words, we can use the unique reduction of the group into its irreducible representations to find a block-diagonal form of the Hamiltonian, with its invariant subspaces having the same dimension as the irreducible representations of the group. Moreover, the number of irreducible representations is equal to the number of equivalence classes in the symmetry group. In the particular case of C_{3v}, the group has three non-trivial irreducible representations of dimension 1 and 2 [typically noted as A_1, A_2, E, with $\dim(A_i) = 1$ and $\dim(E) = 2$]. Consequently, if the defect preserves the original symmetry of the lattice, the defect states are at most double degenerated. In the case of the XS_2-defected monolayers considered in this work, three defect states appear close to the TMDC: a pair of empty in-gap degenerated E states and an occupied non-degenerated A_1 state close to the topmost valence band. Note that the energetics of the defect states cannot be predicted by group theory only, therefore, pointing towards the need of employing *ab initio* methods in the study of these systems.

Van der Waals adsorption of graphene to the TMDC layer lowers the global symmetry of the supercell from C_{3v} to C_s. The C_s symmetry group only has one element apart from the identity E, given by the plane of symmetry and noted σ_s. As a difference to C_{3v}, C_s is Abelian (all the elements of the group commute), and all its irreducible representations are forcibly one-dimensional. Consequently, the eigenenergies and eigenstates of the system are not guaranteed to be degenerated (except for accidental degeneracies). The heterobilayer eigenstates stemming from the former vacancy E states, can now be classified according to one the reflection operators, σ_s. Their different nature is associated to the different size of the anti-crossings between the impurity band and the Dirac cone of graphene. We will use this observation in the calculation of the single-particle rate matrix in Sec. III of the SI.

III. CALCULATION DETAILS FOR $\Gamma^p_{ij}(E, \sigma)$

In this section, we derive an expression for the single-particle rate matrix $\Gamma^p_{ij}(E, \sigma)$ based on the group theory analysis from Sec. II of the SI. We start from Eq. (19), which contains as crucial component the tunneling ("hybridization") matrix elements, $t_{i\mathbf{k}\sigma}$. These matrix elements are assumed to be spin-diagonal, $t_{i\sigma,\mathbf{k}\sigma'} = t_{i\mathbf{k}\sigma}\delta_{\sigma\sigma'}$, as the tunneling occurs over a thin vacuum layer which cannot change the spin orientation. By definition, $t_{i\mathbf{k}\sigma}$ are given

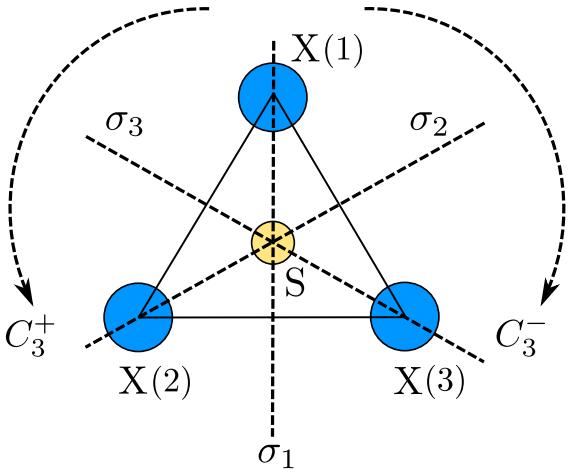

Fig. S1. Schematic representation of the non-trivial operations of the group C_{3v} (rotation by $2\pi/3$, reflection with respect to a plane of symmetry) for the chalcogen vacancy in the XS_2 monolayer.

by

$$t_{i\mathbf{k}\sigma} = \langle i\sigma|\hat{H}|\mathbf{k}\sigma\rangle := \langle i|\hat{H}|\mathbf{k}\rangle, \tag{S1}$$

where $\hat{H}$ is the Hamiltonian of the system, $|i\rangle \equiv |i, \mathbf{0}\rangle$ is a localized impurity state, localized, for convenience, at the origin of the Bravais supercell lattice, $|\mathbf{k}\rangle$ a graphene eigenstate and the spin degree of freedom is kept implicit as it does not intervene in the calculation.

We can express the defect band in the reciprocal space as

$$|i, \mathbf{k}\rangle = \frac{1}{\sqrt{N_{\rm sc}}} \sum_{\mathbf{R}} \mathrm{e}^{\mathrm{i}\mathbf{k}\cdot\mathbf{R}} |i, \mathbf{R}\rangle, \tag{S2}$$

where $\{\mathbf{R}\}$ spans the supercell lattice and $N_{\rm sc}$ is the number of supercell lattice points. It is convenient to have the defect at the origin of coordinates (see Fig. 1 in the main text); then, the inverse transformation reads

$$|i, \mathbf{0}\rangle = \frac{1}{\sqrt{N_{\rm sc}}} \sum_{\mathbf{k}} |i, \mathbf{k}\rangle, \tag{S3}$$

where $\{\mathbf{k}\}$ spans the quasi-momenta lattice of the supercell Brillouin zone.

Using Eq. (19), we estimate the value of the single-particle rate matrix by looking at the region of the spectrum showing level repulsion between the graphene and the vacancy states. Note that we consider only the orbital component of the system without spin-orbit interaction, spin-orbit coupling will be incorporated perturbatively into the model at a later

stage in the main paper. Substituting the matrix elements we find, for each spin sector,

$$\Gamma^{+}_{ij}(E) = \frac{2\pi}{\hbar}\frac{1}{N_{\rm sc}}\sum_{\mathbf{k}}\sum_{\mathbf{k}',\mathbf{k}''}\langle i,\mathbf{k}'|\hat{H}|\mathbf{k}\rangle\langle\mathbf{k}|\hat{H}|j,\mathbf{k}''\rangle\delta(E-\epsilon_{\mathbf{k}}), \tag{S4}$$

$$= \frac{1}{N_{\rm sc}}\sum_{\mathbf{k}}\langle i,\mathbf{k}|\hat{H}|\mathbf{k}\rangle\langle\mathbf{k}|\hat{H}|j,\mathbf{k}\rangle\delta(E-\epsilon_{\mathbf{k}}), \tag{S5}$$

where we used that the graphene and the TMDC layers have the same periodicity. In other words, the translational invariance with respect to the supercell lattice vectors ensures that $t_{i\mathbf{k}\sigma}$ only couples graphene and vacancy states with the same quasi-momentum.

The single-particle tunneling rate matrix is not diagonal in the quasi-angular momentum basis labeled by $i,j=\pm$ because the graphene substrate does not share the same symmetry as the TMDC layer. Instead, as discussed in Sec. II of the SI, in the presence of the graphene layer the TMDC global $\mathrm{C_{3v}}$ symmetry is lowered to a $\mathrm{C_s}$ symmetry. Consequently, we can classify the states by using the action of an operator from the group $\mathrm{C_s}$. For example, we can choose the major plane of symmetry on Fig. 1 whose action on Eq. (S2) is

$$\hat{\sigma}_s|+,\mathbf{k}\rangle = \frac{1}{\sqrt{N_{\rm sc}}}\sum_{\mathbf{R}}\mathrm{e}^{\mathrm{i}\mathbf{k}\cdot\mathbf{R}}|-,\sigma_s\mathbf{R}\rangle = |-,\sigma_s\mathbf{k}\rangle. \tag{S6}$$

Similarly, we find $\hat{\sigma}_s|-,\mathbf{k}\rangle = |+,\sigma_s\mathbf{k}\rangle$. We therefore construct a basis from the quasi-angular momentum states in which $\hat{\sigma}_s$ is diagonal, $\hat{\sigma}_s|u\rangle = u|u\rangle$, with $u=\pm$ from the linear combination (normalized sum/difference) of the $i=\pm$ states. In this basis, $\hat{\sigma}_s|u,\mathbf{k}\rangle = u|u,\sigma_s\mathbf{k}\rangle$ and $\hat{\sigma}_s|\mathbf{k}\rangle = \exp[i\varphi(\mathbf{k})]|\sigma_s\mathbf{k}\rangle$ where $\varphi(\mathbf{k})$ is a phase. We now show that Eq. (S5) is a diagonal matrix in this basis, which also defines a symmetry of the Hamiltonian $\hat{H}$. Using the observations above, it is straightforward to prove that

$$\sum_{\mathbf{k}}\langle u,\mathbf{k}|\hat{H}|\mathbf{k}\rangle\langle\mathbf{k}|\hat{H}|\bar{u}\mathbf{k}\rangle = \sum_{\mathbf{k}}\langle u,\mathbf{k}|\hat{\sigma}_s^2\hat{H}\hat{\sigma}_s^2|\mathbf{k}\rangle\langle\mathbf{k}|\hat{\sigma}_s^2\hat{H}\hat{\sigma}_s^2|\bar{u}\mathbf{k}\rangle = -\sum_{\mathbf{k}'}\langle u,\mathbf{k}'|\hat{H}|\mathbf{k}'\rangle\langle\mathbf{k}'|\hat{H}|\bar{u},\mathbf{k}'\rangle, \tag{S7}$$

with $\mathbf{k}'=\sigma_s\mathbf{k}$ and $\bar{u}=-u$. Here, we used that the phase $\varphi(\mathbf{k})$ cancels out into the projector $|\mathbf{k}\rangle\langle\mathbf{k}|$. As a consequence $\Gamma^{+}_{u\bar{u}} = -\Gamma^{+}_{u\bar{u}} = 0$, i.e. the single-particle rate matrix is diagonal in the orbital subspace, $\Gamma_{uu'} = \Gamma^{+}_{uu}\delta_{uu'}$ with $\Gamma^{+}_{uu'} = \Gamma^{-}_{u'u}$.

We thus consider only the diagonal elements,

$$\Gamma^{+}_{uu}(E) = \frac{2\pi}{\hbar}\frac{1}{N_{\rm sc}}\sum_{\mathbf{k}} |\langle u,\mathbf{k}|\hat{H}|\mathbf{k}\rangle|^2 \delta(E-\epsilon_{\mathbf{k}}), \tag{S8}$$

and, in the limit $N_{sc}\to\infty$, we transform the discrete sum over the quasimomenta into an integral over the supercell Brillouin zone by

$$\sum_{\mathbf{k}} \to \frac{N_{\rm sc}A_{\rm sc}}{(2\pi)^2}\int_{\rm SBZ} {\rm d}\mathbf{k}, \tag{S9}$$

where A_{sc} is the supercell area. Thus, Eq. (S8) becomes

$$\Gamma_{uu}(E) = \frac{2\pi}{\hbar}\frac{A_{\rm sc}}{(2\pi)^2}|t_u|^2\sum_{\tau}\int_0^{2\pi} d\varphi \int_0^{\infty} dk k\delta(E-\hbar v_{\rm F}k), \tag{S10}$$

where $\tau=\pm$ is the valley index, $v_{\rm F}$ the Fermi velocity and k measures the distance of the quasi-momentum from a graphene Dirac point. Moreover, $t_u := t_{u\mathbf{k}\sigma}$ is defined as in Eq. (S1) and we dropped the $\pm$ superindex as the matrix is diagonal. Notice that the integral has been extended to $k\to+\infty$, which can be justified by the δ function, as far as E is sufficiently close to the graphene charge neutrality point.

Introducing the graphene unit cell, $A_{\rm c}$ and density of states close to its pristine chemical potential, $\rho_{\rm Gr}(E) = 2A_c|E|/(\pi\hbar^2 v_{\rm F}^2)$, we obtain the diagonal elements of the single-particle rate matrix in their final form

$$\Gamma_{uu}(E) = \frac{\pi^2}{2\hbar}\frac{A_{\rm sc}}{A_{\rm c}}|t_u|^2\rho_{\rm Gr}(E). \tag{S11}$$

The final step consists in estimating the absolute value of the hybridization matrix elements, which can be done by employing Eq. (23) in the main text in the context of avoided crossings in a local two-level system.

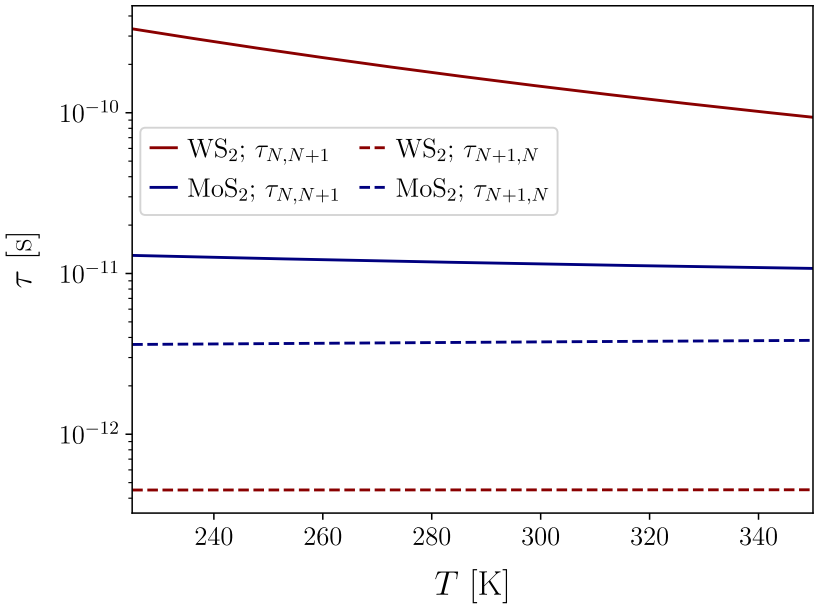

Fig. S2. Electronic transition time, τ, for MoS_2 and WS_2 vacancy states as a function of bath temperature, T measured in kelvin, for the transitions $\alpha \to \beta$ with $\alpha, \beta \in \{N, N+1\}, \alpha \neq \beta$.

IV. TEMPERATURE AND DEFECT ENERGY DEPENDENCE OF THE MANY-BODY TRANSITION RATES

We display in Fig. S2 the transition times evaluated for a wide range of bath temperatures at fixed chemical potential (here $\mu = 0$). For this temperature, well within the weak coupling limit $\hbar\Gamma \ll k_B T$, the transition rates are very smooth functions. Temperature opens (or closes) the window around the defect energies where the transition to and from the reservoir can be active, and therefore, larger sensitivity to temperature is expected in WS_2 compared to MoS_2 because its defect levels are further from the Fermi energy of undoped graphene. In addition, as we are essentially observing the effect of temperature on the Fermi function, similar behavior occurs for the case of strong spin-orbit interaction by evaluation of Eqs. (39)-(41).

In Figs. S3 and S4, we show the change in the transition time when the position of the defect levels with respect to the charge neutrality point is rigidly shift. We assume that this shift is not too large so that the hybridization matrix elements remain constant. This type of level shift can be used to understand the impact of the change of the position of the defect levels in the transition rates at lowest order, if screening would be taken into consideration, *e.g.* at the G_0W_0 level. We consider first on the case of weak spin-orbit interaction. Overall,

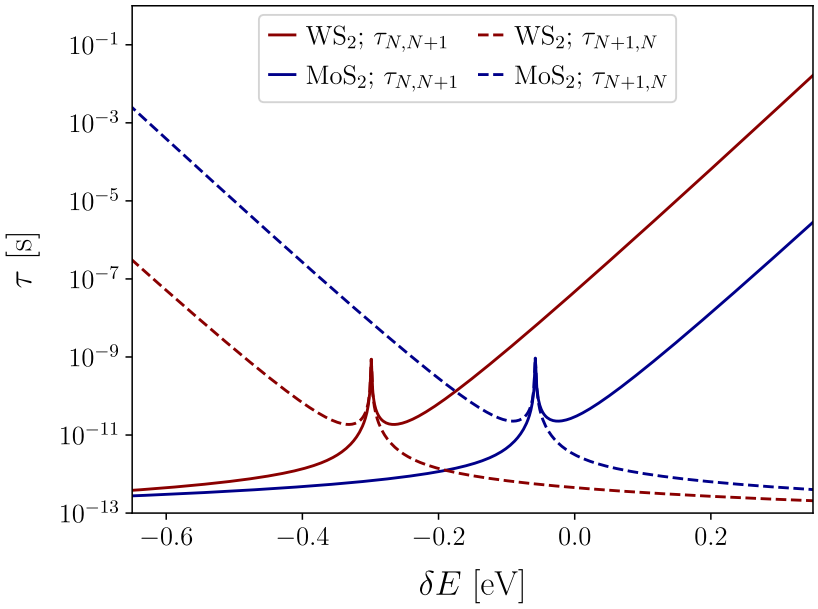

Fig. S3. Electronic transition times, τ, for MoS_2 and WS_2 vacancy states as function of the shift of the defect levels, δE, given in eV and measured from $\mu = 0$. This shift would result from *e.g.* including screening effects. The solid and dashed lines correspond to the transitions $N \to N+1$ and $N+1 \to N$ respectively.

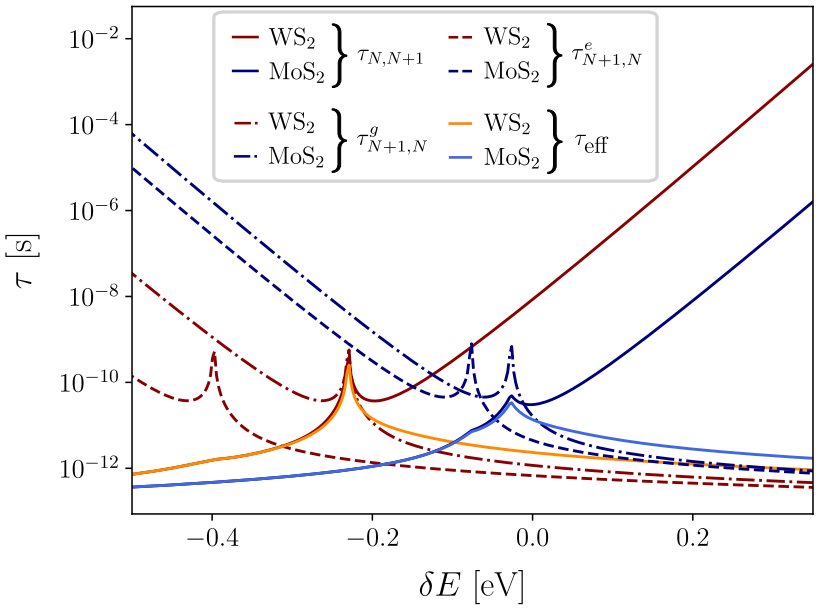

Fig. S4. Electronic transition times with spin-orbit interaction, τ, for vacancy states at the MoS_2–Gr and WS_2–Gr interface as function of the shift of the defect levels, δE, given in eV and measured from $\mu = 0$. This shift would result from *e.g.* including screening effects. The solid and dashed lines correspond to the transitions $N \to N+1$ and $N+1 \to N$ respectively.

we observe that the trends corresponding to the charging and discharging processes are reversed when comparing to the trends in Fig. 5 (a). For example, the charging of the vacancy becomes slower when the energy levels are shifted away from the charge neutrality point, while the discharging becomes faster. In other words, the positive rigid shift that would occur if screening would be included works in the opposite way as the positive gate voltage (as the pristine band gap becomes larger). In addition, a cusp over the smooth trends is present once the defect levels are shifted towards the graphene Dirac point. This cusp is originated by the alignment of the defect energy with the energy at the $\bar{\mathrm{K}}$ point, $\delta E = -\Delta E_{0,u}$, where the inverse DoS acquires a non-analytical scaling as $\sim |E|^{-1}$. While an enhancement of the relaxation time should be expected due to these phase space arguments, its divergence is an artefact of the perturbative approach. For example, when considering the tunnelling coupling in the dressed second order approximation[10], the tunnelling rate for a given many-body transition is obtained by convolution of the DoS with a Lorentzian centered on the resonant energy, thus preventing exact vanishing of the rate. In Fig. **??** we present the electronic transition times in presence of SOC. The transition times to the single energy levels are still characterized by the diverging cusp, which is smoothed in τ_{eff}, as the effective rate never vanishes due to the contribution of both energy levels. Evidently, at the $\mathrm{G_0W_0}$ level the precise value of δE is fixed once the screening conditions are determined, but the numerical simulations suggest both an additional way of modifying the transition rates if the dielectric environment is altered in a controlled way and a manner of interpret and understand screening from the experimentally measured transition rates.

---

[1] P. Giannozzi, S. Baroni, N. Bonini, M. Calandra, R. Car, C. Cavazzoni, D. Ceresoli, G. L. Chiarotti, M. Cococcioni, I. Dabo, A. Dal Corso, S. de Gironcoli, S. Fabris, G. Fratesi, R. Gebauer, U. Gerstmann, C. Gougoussis, A. Kokalj, M. Lazzeri, L. Martin-Samos, N. Marzari, F. Maurim, R. Mazzarello, S. Paolini, A. Pasquarello, L. Paulatto, C. Sbraccia, S. Scandolo, G. Sclauzero, A. P. Seitsonen, A. Smogunov, P. Umari, and R. M. Wentzcovitch, Journal of Physics: Condensed Matter **21**, 395502 (2009).

[2] J. P. Perdew, K. Burke, and M. Ernzerhof, Phys. Rev. Lett. **77**, 3865 (1996).

[3] M. J. van Setten, M. Giantomassi, E. Bousquet, M. J. Verstraete, D. R. Hamann, X. Gonze,

and G.-M. Rignanese, Computer Physics Communications **226**, 39 (2018).

[4] G. Kresse and J. Furthmüller, Phys. Rev. B **54**, 11169 (1996).

[5] O. A. Vydrov and T. Van Voorhis, The Journal of Chemical Physics **130**, 104105 (2009).

[6] K. Berland, V. R. Cooper, K. Lee, E. Schröder, T. Thonhauser, P. Hyldgaard, and B. I. Lundqvist, Reports on Progress in Physics **78**, 066501 (2015).

[7] E. P. Wigner, *Group Theory and its Application to the Quantum Mechanics of Atomic Spectra*, 1st ed. (Academic Press, 1959).

[8] M. S. Dresselhaus, G. Dresselhaus, and A. Jorio, *Group Theory: Applications to the Physics of Condensed Matter* (Springer, 2008).

[9] F. Cotton, *Chemical Applications of Group Theory*, 3rd ed., Wiley-Interscience publication (Wiley, 1990).

[10] J. Kern and M. Grifoni, The European Physical Journal B **86**, 384 (2013).